IJE TRANSACTIONS B: Applications Vol. 27, No. 5, (May 2014) 785-792

International Journal of Engineering

Journal Homepage: www.ije.ir

An Outrun Competition of Corrosion Fatigue and Stress Corrosion Cracking on Crack Initiation in a Compressor Blade

E. Poursaeidi*, O. Pedram

Department of Mechanical Engineering, University of Zanjan, Zanjan, Iran

PAPER INFO

Paper history:
Received 25 June 2013
Received in revised form 24 August 2013
Accepted 07 November 2013

Keywords:
Corrosion Pitting
Gas Turbine Compressor Blade
Stress Corrosion Cracking
Custom 450

ABSTRACT

The first row rotating blades of four axial-flow compressors fractured prematurely. Previous investigations had shown that the atmosphere of the site contained corrosive compounds which lead to an increase in possibility of pitting of the blades. It was also revealed that the crack was originated from two corrosion pits. Thus, this work is conducted to ascertain which of the fatigue or stress corrosion cracking (SCC) mechanisms is predominant in transition of pits into initial cracks. To this end, experimental, numerical and theoretical studies are considered. Replica testing, Scanning Electron Microscope (SEM) and fractography of the broken blade indicate that the pits join together and make one bigger pit under SCC mechanism which reduces the failure time. 3-D models of the pitting on the blade under existing forces are analyzed by ABAQUS software. The simulation results show the location of maximum stress concentration inside one of the pits which is compatible with the location of initial SCC crack. Theoretical and numerical analysis show that stress intensity range (ΔK) around the pits is smaller than threshold stress intensity range (ΔK_{th}); thus, cracks initiate and propagate at the mouth of the pits under SCC mechanism. Then, the pits join together and make one equivalent pit, so that ΔK reaches the ΔK_{th} and finally crack propagates under fatigue mechanism.

doi: *10.5829/idosi.ije.2014.27.05b.15*

1. INTRODUCTION

Initiation and growth of cracks depend on different reasons and conditions [1, 2]. One of these reasons and conditions is Pitting corrosion. Pitting corrosion is defined as "localized corrosion of a metal surface, confined to a point or small area that takes the form of cavities" [3]. It is a deleterious form of localized corrosion which mainly occurs on metal surfaces and owes their corrosion resistance to passivity. Pitting corrosion is very complicated in nature because "oxide films formed on different metals vary one from another in electronic conduction, porosity, thickness, and state of hydration" [4]. Therefore, how and when pitting occurs on a metal depends on numerous factors, such as type of alloy, its composition, integrity of its oxide film, presence of any material or manufacturing-induced discontinuities, and chemical and loading environment.

*Corresponding Author Email: epsaeidi@znu.ac.ir (E. Poursaeidi)

Stress corrosion failures are comparatively rare; the consequences can be severe and occasionally catastrophic though. Consequently, considerable efforts focus on evaluation of effects of operational variables on pitting and crack growth and developing an improved basis for structural integrity assessment. Whilst localized straining is undoubtedly important, the kinetics of reactions depend on the local chemistry and potential, and variations of them within the pit can also play a role. Thus, the factors determining the crack evolution process are very complex [5-8].

During the past two decades, researchers have strived to develop mechanistic or physics-based model to understand and predict SCC and corrosion fatigue (CF). However, so farno specific model is completely agreed upon. Many of these models are postulated on the premise of rigorous experimental data. The active path dissolution and film rupture model and hydrogen assisted cracking model are the two most popular among SCC/CF research community [9]. Saito and

Kuniya [10] present a predictive methodology for SCC crack growth using a mechanochemical model based on a slip formation/dissolution mechanism. The mechanochemical model consists of the combined kinetics of the plastic deformation process as a mechanical factor and slip dissolution-repassivation process as an environmental factor at a crack tip. The theoretical predictions according to the mechanochemical model are quantitatively in good agreement with many experimental observations of the effect on SCC crack growth for type 304 SS in 288°K water.

Pits can serve as initiation sites for SCC. A well-developed model for the transition from pitting to SCC has not been developed; however, a model for the initiation of CF cracks at pits does exist. In the model discussed by Hagn [11], pits are regarded as half-elliptical surface cracks since they have tiny fissures at their bottoms. Though this expression was discussed in the context of CF, he claims that it is also applicable to SCC.

Liu and Macdonald [12] indicate that for $K_I \le K_{ISCC}$, (K_I) is stress intensity factor of mode I, K_{ISCC} is threshold stress intensity factor of mode I for SCC condition and K_{IC} is plane strain fracture toughness) the crevice develops by pitting corrosion, but when $K_I = K_{ISCC}$, a stress corrosion cracking initiates. The crack then propagates over $K_{ISCC} \le K_I \le K_{IC}$ by environmental-assisted fracture, but when $K_I \ge K_{IC}$, the crack leads to fast fracture (failure).

In the presence of corrosive media, accelerated fatigue failure can occur due to the well-known mechanochemical and chemomechanical interactions. It is well known that plastic deformation can accelerate the anodic dissolution of metals and promote CF crack initiation and propagation. One of the main failure mechanisms for CF is that cracks usually initiate at pits [13]. The effect of pitting on fatigue is not yet well understood. This may be due to the lack of understanding of the interaction between defects and electrochemical reactions on pitting [14]. Nakajima and Tokaji [15] perceived that a crack emanates from a pit during simultaneous corrosion fatigue only if the pit grows to such a level that the stress-intensity factor reaches a certain threshold value. To quantify pitting induced corrosion fatigue, a critical pit size model and a pitting/cracking competition model were proposed to characterize the corrosion fatigue crack nucleation process [16].

A prevalent premature fracture failure in first row rotating blades of gas turbine compressors installed in a seaside power plant had been observed. Previous studies [17-19] revealed that the failures were due to crack propagation from initial surface pits under high cycle fatigue mechanism. Following the previous investigations, this paper focuses on fractured blade of one of the compressors to determine the predominant mechanism (CF or SCC) in transition of pits into initial cracks.

2. EXPERIMENTS AND OSERVATIONS

2. 1. Physical Inspections The fracture on the failed blade occurred 62 mm above the hub of the blade. Figure 1a shows the fractured blade and its position in the first row of the gas turbine compressor, before detaching from the system. Figure 1b shows brown points as an index of corrosion or corrosion pitting signs

2. 2. Chemical Analysis Regarding chemical analysis [17], the blade was conformed to AISI Custom 450. It is an age-hardenable martensitic stainless steel. It has the strength characteristics of a martensitic stainless steel combined with a corrosion resistance comparable to an 18Cr-8Ni stainless. Its good corrosion resistance derives from a composition which includes 15% Cr, 6% Ni and 0.8% Mo [20]. Its strength and corrosion-resistance properties among the other stainless steels are shown in Figure 2.

Energy Dispersive Analysis by X-ray (EDAX) revealed that there were some abnormal elements such as Chlorine, Natrium and Phosphorus in the pitting places. Result of EDAX is shown in Figure 3.

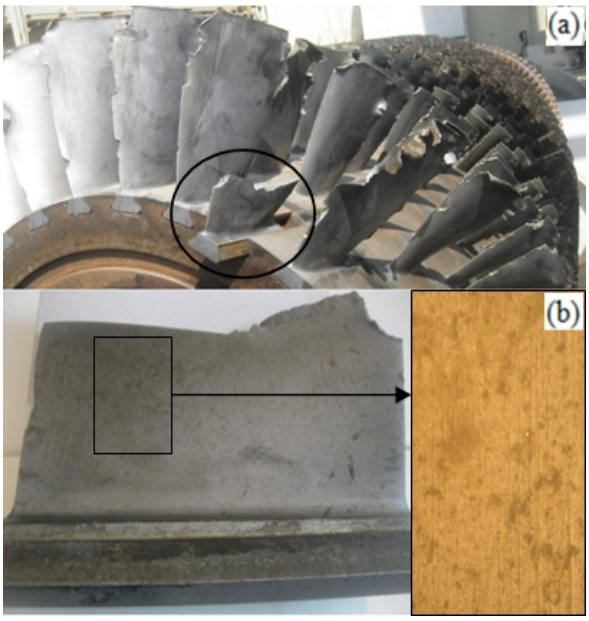

Figure 1. (a) Fractured blade and its position, (b) Brown points as an index of corrosion or corrosion pitting signs

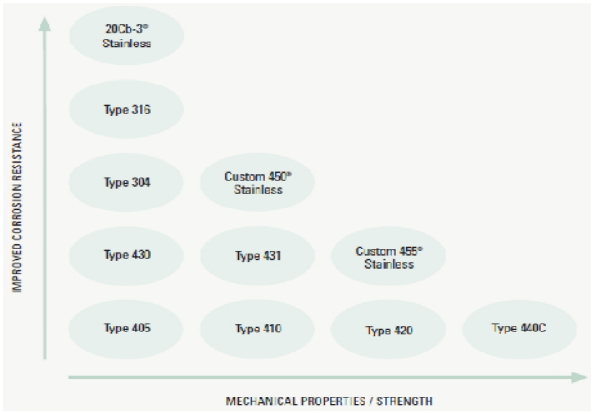

Figure 2. Comparison of corrosion resistance versus strength for Custom 450 and other stainless steels [21]

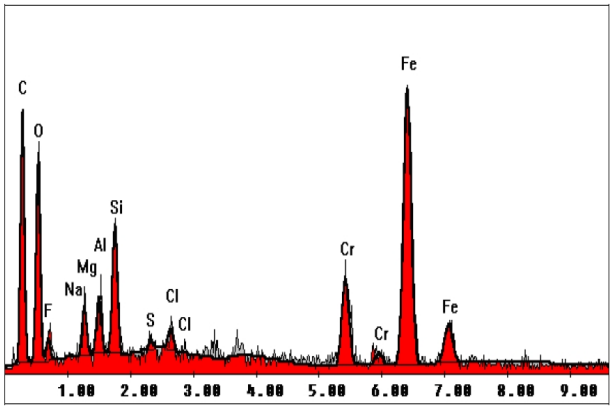

Figure. 3. EDAX at the pits showing high amount of F, Na, Si, S and Cl elements

2. 3. Fractography and SEM Investigations Figure 4a shows the state of the fractured blade. Except for a small part on the corner of the blade leading edge (final fractured area in Figure 4a), the fractured surface is undamaged. The two small pits existing on the edge of fractured surface are the source of crack initiation. Through the magnified image of Figure 4b, two semi-elliptical regions can be seen that show fatigue crack growth. In this figure, recognition of beach marks in macroscopic scale is possible. The bigger semi-elliptic dominates in crack development and so determines the critical state of fracture. To see the crack initiation points better and also study the stress corrosion cracking phenomenon, replica examination was carried out (Figure 4a). A typical intergranular micro crack is seen as SCC in Figure 5a. Figure 5b (the magnified image of the first crack initiation area in Figure 4b) shows how two adjacent pits, A and B, are joined under SCC mechanism and make one equivalent semi-elliptical pit. The other SCC crack starts from the base of equivalent corrosion pit. In Figure 4b, pits A and B are in the first crack origin and the location of initiation of SCC and bigger semi elliptical fatigue crack. In Figure 5b, $a = 15\mu m$ and $c = 20\mu m$ are the dimensions of half of the vertical and horizontal diameters of the equivalent semi elliptical pit, respectively.

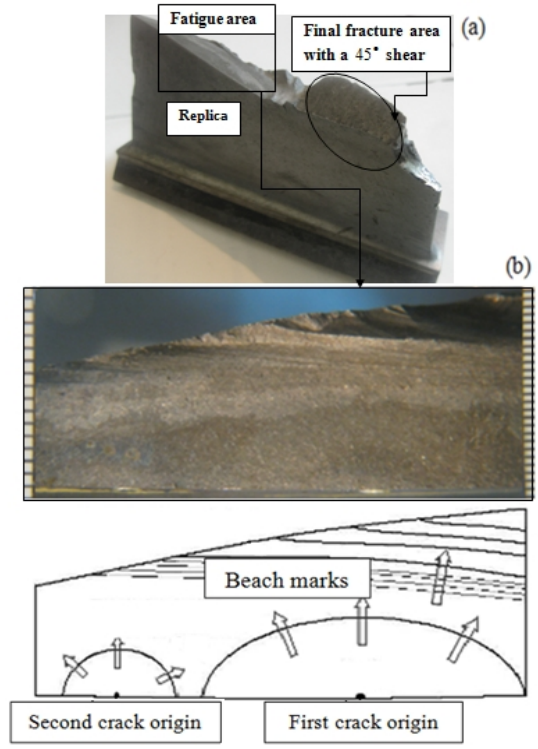

Figure 4. (a) State of failed blade, (b) Magnified view of fractured surface and growth of fatigue crack

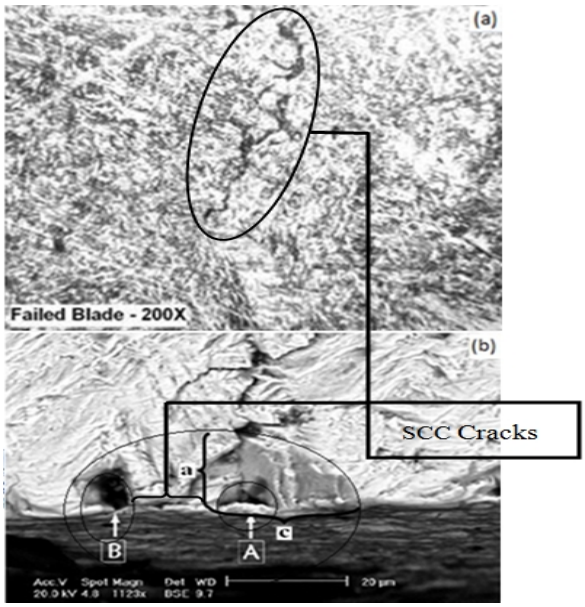

Figure 5. (a) Intergranular SCC cracks, (b) Formation of SCC between two pits and making equivalent semi elliptical pit

3. SIMULATION OF PITS AND FINITE ELEMENT ANALYSIS

To calculate the stresses on blade surface, the model of blade airfoil and hub is constructed using SolidWorks software and it is imported to ABAQUS for simulation. Afterwards, essential mechanical properties based on Table 1 are defined to software. Since the blade in disk slot has relatively rigid connection, displacement and rotation of blade root are constrained in all directions.

The mesh is created using the 102487 disciplined 3D elements C3D10 which are of 10-node quadratic tetrahedral types (Figure 6a). Three kinds of forces act on the blade. A 5163 RPM rotational speed that produces statically centrifugal force, 116.6 Nm aerodynamic torsion moments, and static pressure that is like trapezoid varying from tip to hub on the blade pressure side as shown in Figure 6b.

TABLE 1. Mechanical Properties of GTD 450 [22, 23]

Property	Magnitude
Poisson's Ratio, υ	0.29
Modulus of Elasticity, E [GPa]	200
Density, ρ [kg/m^3]	7800
Yield strength, YS (MPa)	1296
Ultimate strength, UTS (MPa)	1351
Fracture toughness, K_{IC} ($MPa\sqrt{m}$)	78

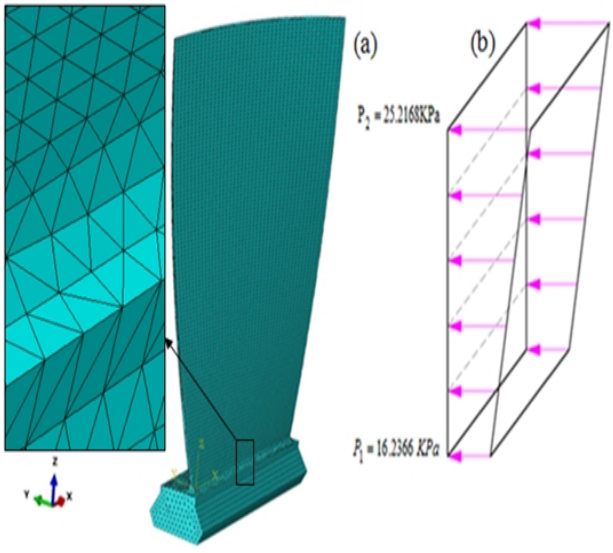

Figure 6. (a) Meshed blade model, (b) Pressure distribution on the pressure side of blade

First, static analysis is done to find how much tensile stress exists on the fractured surface at the location of crack origin. Most of this tensile stress is owing to centrifugal load. Figure 7 shows principal stress distribution along the z-axis (longitudinal axis of the blade). The tensile stress at the location of crack initiation on pressure surface of blade is 170 MPa. It is seen that the maximum stress of 170 MPa is below the yield strength of Custom 450 (Table 1), so that the blade can withstand the forces under static condition without existence of principal crack. Measurements are taken to the fractured blade in the second model. Region of origin location of SCC crack between two adjacent pits A and B, in fractured section (Figure 5b), is shown using "red cross" in Figure 8.

One of the paramount important points in pit or pits modeling is considering their relative size and position. It means that it is not required to preserve the exact sizes and distances. Thus, by considering the relative distances and scale, we can reach exactly the same results with the actual size of the model. Since the size of pits A and B are so small, it is preferred to utilize the relative simulation based on the size used by Haskel[20] in evaluation and determination of the effects of them on stress concentration.

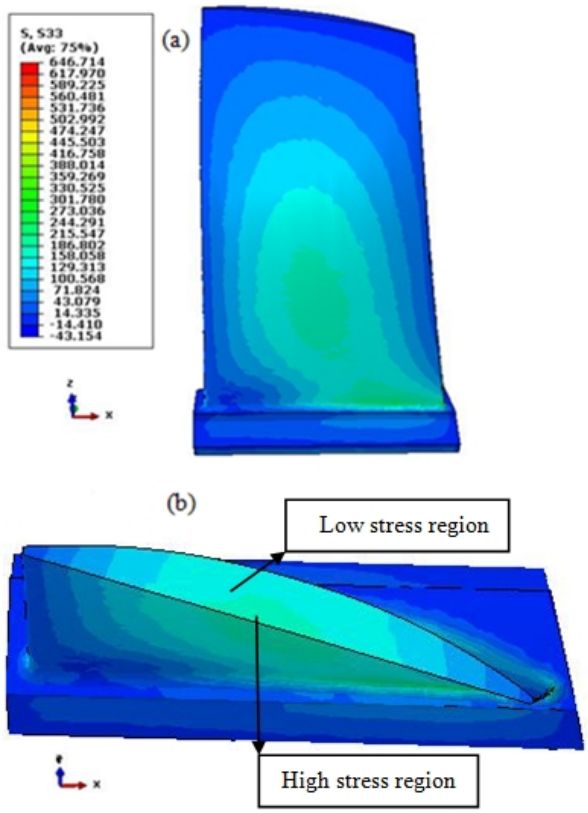

Figure 7. Principal stress distribution along the z-axis on the pressure surface of the blade under static loads (a) Entire blade, (b) Fractured section

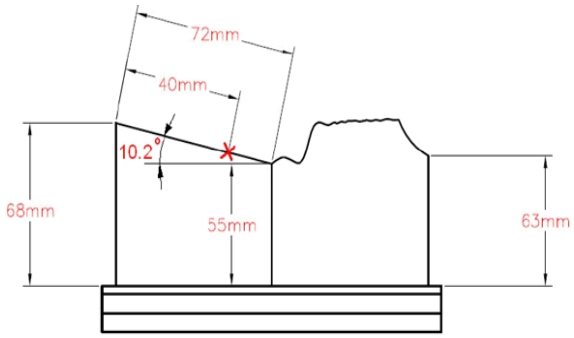

Figure 8. Schematic of front view of the fractured blade with some dimensions and main pit position

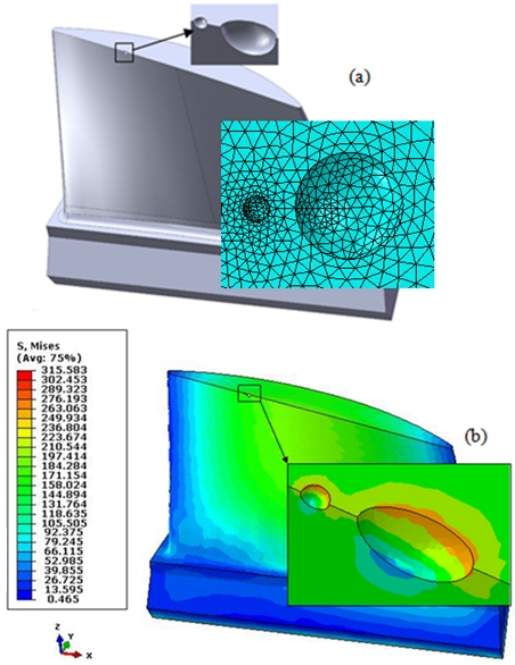

Figure 9. (a) Simulation of two adjacent pits and mesh distribution in the blade geometry, View of the fractured surface, (b) Principal stress distribution along the z-axis under static loads at the mouth and the bottom of pits

Figure 9 shows principal tensile stress distribution at fractured surface. Stress concentration area is obvious at the mouth and depth of the pits which are the locations of the aforementioned fatigue and SCC crack initiation sites. The pits increase tension by approximately 50 MPa.

Yellow region with stress of approximately 200 MPa between two pits, indicates their interaction in the operating conditions of the compressor blade. This can be extended to the mutual influence of two adjacent origin cracks (the first and the second origin cracks) in Figure 4b. Two semi-elliptic cracks grow in this high stress region and cause beach marks interaction as happened in Figure 4b.

The stress distribution shows the expected behavior in high stress region around the bottom and mouth of the pit. Finite element analysis results show reasonable agreement with the experimental observations (Figure 4 and Figure 5).

4. TRANSITION OF PITS INTO INITIAL CRACKS

Regarding the fractured surface (Figure 5), the crack firstly initiates from the pits under intergranular stress corrosion cracking mechanism, but later on due to fatigue nature of fractured process, transgranular crack growth dominates.

The higher the yield strength of a high strength stainless, the more susceptible it will be to stress corrosion cracking [21]. High-strength materials can be cracked due to hydrogen embrittlement. Hydrogen sulfide and chloride in the environment can be the cause of stress corrosion cracking of the alloy [24]. Custom 450 is a high-strength alloy and existence of unusual elements like Sulfur, Potasium, Chloride and moisture in the site increases the possibility of stress corrosion cracking. Based on [25], fractography properties of SCC crack shown in Figure 5, is in good agreement with two mechanisms of active path and hydrogen embrittlement.

Using the diagram provided for Custom 450 [26], a relationship between time (t) and pit depth (x) under similar working conditions (CF), using a curve fitting tool is obtained:

$$x = 37.66 \times t^{0.47} - 43.72 \quad (1)$$

where, time is in month, and depth of the pit is in micrometer. Now, using Equation (1), the time for pits A, B and equivalent pit formation, according to the dimensions indicated in Figure 5b, is calculated:

$$t_A = 3.59 \ monthes$$
$$t_B = 4.80 \ monthes$$
$$t_{eq} = 11.51 \ monthes$$

According to Figure 5, time for SCC crack formation between pit A and B and their joining together (t_{SCC}), can be calculated as follows:

$$\frac{da}{dt_{SCC}} = C(K_{ISCC})^n \quad (2)$$

In which,

$$K_{ISCC} = 1.12\sigma\sqrt{\pi a} \quad (3)$$

where, a is SCC crack length and σ is constant tensile stress at SCC crack region which is equal to 200 MPa

(Figure 9b). So, K_{ISCC} is calculated.

$$K_{ISCC}= 3.44 MPa\sqrt{m}$$

Using C and n for Paris law [17] and integrating along the SCC crack length, this time is calculated.

$$t_{SCC} = 4.20 \quad monthes$$

On the other hand, using the Lindley relation [27], stress intensity factor range for fatigue crack initiation from corrosion pit (pit A (ΔK_A), pit B (ΔK_B) and equivalent pit (ΔK_{eq})) can be calculated as follows:

$$\Delta K = \frac{\Delta\sigma\sqrt{\pi a[1.13 - 0.07(a/c)^{1/2}]}}{\left[1 + 1.47(a/c)^{1.64}\right]^{1/2}} \quad (4)$$

In Equation (4), $\Delta\sigma$ is dynamic stress that causes fatigue which is equal to 118 MPa.

$$\Delta K_A = 0.75 MPa\sqrt{m}$$
$$\Delta K_B = 0.67 MPa\sqrt{m}$$
$$\Delta K_{eq} = 1.35 MPa\sqrt{m}$$

By comparing the values of stress intensities, it can be concluded that first SCC happens and joins pit A and B. So, the equivalent pit is made. Formation of equivalent pit causes the stress intensity to reach threshold value and crack to start under the corrosion fatigue mechanism. That is, none of the pits A and B have not the ability to transform into fatigue cracks before the equivalent pit is formed.

According to the times calculated for pit and SCC crack growth, it is clear that the time for small pits to grow up to the size of equivalent pit in the absence of the SCC phenomena is about twice that of the time for SCC crack between pits A and B to occurs and make the equivalent pit. Thus, the occurrence of SCC at the location of pit reduces the crack initiation life to half.

To study the initiation and growth of cracks from equivalent pit, Figure 10 is schematically drawn. Cyclic stress and more of its effect on the location of stress concentration cause fatigue crack to initiate from the mouth of the pit. After some fatigue cycles, the crack depth is almost the same as the pit depth. Two quarter-elliptical crack from two sides of the pit (Figure 10b) grow and in pit depth join together to form a semi-elliptical crack.

For a crack initiated from a shallow pit, it is assumed that the initial elliptical crack with depth of pit grows to be a semicircular shape crack (short crack), as shown in Figures 10c and 10f, and then this semicircular crack grows into a final elliptical one (long crack), as shown in Figure 10d [14]. Stress corrosion cracking is created at the pit depth due to the presence of the stressful area and corrosive products.

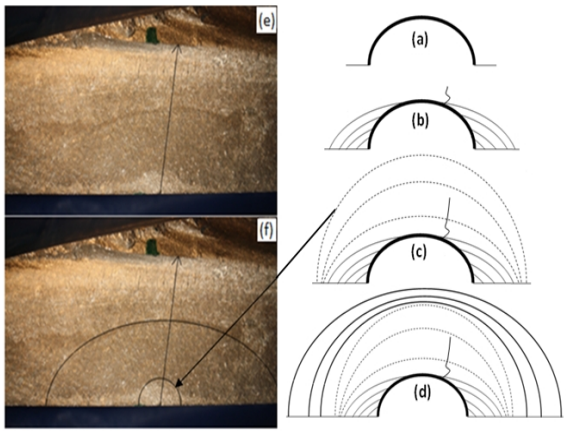

Figure 10. Steps of crack growth from equivalent pit

Stress decreases by moving to the depth at cross section of fractured surface (Figure 7b). That the reason that SCC has stopped gradually and the fatigue crack has overcome, so SCC does not influence the failure and life of the blade.

Plastic deformation at the edge of fractured surface where final fracture begins, shows that tensile and bending loading at this stage is overloaded. In fact, with the fatigue crack growth, the remaining surface area becomes smaller, and when the size of the crack reaches the critical value, so remained surface suddenly fails.

5. CONCLUSION

First row rotating blades of four axial-flow compressors were fractured before the due date. Previous investigation showed that the crack was initiated from surface pits.

Because of high tensile stress, corrosive environment and existence of Hydrogen, Chlorine and Sulfur that cause corrosion pits on high strength blade surface, the possibility of SCC soars.

SEM shows two adjacent pits are joined and make one equivalent semi-elliptical pit.

By using finite element analysis, stresses around the pits are calculated. Then, the critical stress intensity factors at the pits region for both CF and SCC conditions are determined. According to the above results, it is found that the SCC has grown from pit A and B and corrosion fatigue starts from the equivalent pit.

Finite element analysis shows good similarities with fractography photos. Stress concentration and interaction of stresses around the pits are two mechanical reasons for initiation and growth of cracks.

Calculations show that the occurrence of SCC at the location of the pit reduces the crack initiation time to half.

6. ACKNOWLEDGEMENT

The authors would like to thank Mr. M. Arablu and Mrs. M. Pedram for the article editorial helps.

7. REFERENCES

1. Majzoubi, G. H. And Farahi, G. H., "Crack Behavior Of The Aluminum Alloy 2024 Under Fretting Conditions", ***International Journal of Engineering***, Vol. 15, (2002), 287-292.
2. Mohajerani, A. and Farrahi, G., "numerical investigation of crack orientation in the fretting fatigue of a flat rounded contact", ***International Journal of Engineering-Transactions B: Applications***, Vol. 23, No. 3&4, (2010), 223-230.
3. American Society for Metals (ASM), "Metals Handbook, Corrosion, 9th edition, Metals Park, Ohio, USA, Vol. 13, (1987).
4. Jayalakshmi, M. and Muralidharan, V., "Empirical and Deterministic Models of Pitting Corrosion-An Overview", ***Corrosion Reviews***, Vol. 14, No. 3-4, (1996), 375-402.
5. Turnbull, A., Horner, D. and Connolly, B., "Challenges in modelling the evolution of stress corrosion cracks from pits", ***Engineering Fracture Mechanics***, Vol. 76, No. 5, (2009), 633-640.
6. Turnbull, A., McCartney, L. and Zhou, S., "A model to predict the evolution of pitting corrosion and the pit-to-crack transition incorporating statistically distributed input parameters", ***Corrosion science***, Vol. 48, No. 8, (2006), 2084-2105.
7. Turnbull, A., Wright, L. and Crocker, L., "New insight into the pit-to-crack transition from finite element analysis of the stress and strain distribution around a corrosion pit", ***Corrosion Science***, Vol. 52, No. 4, (2010), 1492-1498.
8. Horner, D., Connolly, B., Zhou, S., Crocker, L. and Turnbull, A., "Novel images of the evolution of stress corrosion cracks from corrosion pits", ***Corrosion Science***, Vol. 53, No. 11, (2011), 3466-3485.
9. Mohanty, S., Majumdar, S. and Natesan, K., "A Review of Stress Corrosion Cracking/Fatigue Modeling for Light Water Reactor Cooling System Components", (2012).
10. Saito, K. and Kuniya, J., "Mechanochemical model to predict stress corrosion crack growth of stainless steel in high temperature water", ***Corrosion Science***, Vol. 43, No. 9, (2001), 1751-1766.
11. Hagn, L., "Lifetime prediction for parts in corrosive environments", ***Corrosion in Power Generating Equipment***, (1983), 481-516.
12. Liu, C. and Macdonald, D., The deterministic prediction of damage functions to low pressure steam turbines., Pennsylvania State Univ., University Park, PA (United States). Center for Advanced Materials. (1993)
13. Ma, J., Zhang, B., Wang, J., Wang, G., Han, E.-H., and Ke, W., "Anisotropic 3D growth of corrosion pits initiated at MnS inclusions for A537 steel during corrosion fatigue", ***Corrosion Science***, Vol. 52, No. 9, (2010), 2867-2877.
14. Rokhlin, S., Kim, J.-Y., Nagy, H. and Zoofan, B., "Effect of pitting corrosion on fatigue crack initiation and fatigue life", ***Engineering Fracture Mechanics***, Vol. 62, No. 4, (1999), 425-444.
15. Nakajima, M. and Tokaji, K., "A Mechanical Condition of Fatigue Crack Initiation from Corrosion Pits", in In Fatigue'96, Proceedings of the Sixth International Fatigue Congress, Berlin, Germany. (1996), 697-702.
16. Chen, G., Wan, K.-C., Gao, M., Wei, R. and Flournoy, T., "Transition from pitting to fatigue crack growth—modeling of corrosion fatigue crack nucleation in a 2024-T3 aluminum alloy", ***Materials Science and Engineering: A***, Vol. 219, No. 1, (1996), 126-132.
17. Poursaeidi, E., Sanaieei, M. and Bakhtyari, H., "Life Estimate of a Compressor Blade through Fractography", ***International Journal of Engineering***, Vol. 26, No. 4, (2013).
18. Poursaeidi, E., Babaei, A., Behrouzshad, F. and Mohammadi Arhani, M., "Failure analysis of an axial compressor first row rotating blades", ***Engineering Failure Analysis***, Vol. 28, No., (2013), 25-33.
19. Poursaeidi, E. and Arablu, M., "Humidity Effects on Corrosion-Assisted Fatigue Fracture of Heavy-Duty Gas Turbine Compressor Blades", ***Journal of Propulsion and Power***, Vol. 29, No. 5, (2013), 1009-1016.
20. Haskell, R., "Gas turbine compressor operating environment and material evaluation", in R. W. Haskell, ASME, Gas Turbine and Aeroengine Congress and Exposition, Toronto, Canada. Vol. 13, (1989).
21. Alloys, C. S., "Alloys for Corrosive Environments", ***CRS Holdings In***, Vol. U.S.A. 7-03/2.5M, , (2003).
22. Mansur, A., "Modeling of mechanical properties of ceramic-metal composites for armor applications", University of Ottawa, (2011),
23. Midha, A. and Wert, D. E., "Martensitic Age-Hardenable Stainless Steel", ***Advanced Materials & Processes***, Vol. 169, No. 9, (2011), 30-33.
24. Cottis, R., "Guides to Good Practice in Corrosion Control—Stress Corrosion Cracking", ***National Physical Laboratory, Teddington***, (2000).
25. Gulbrandsen, S., "Overview of Stress Corrosion Cracking in Stainless Steel: Electronic Enclosures in Extreme Environmental Conditions",
26. Linden, D., "Long Term Operating Experience with Corrosion Control in Industrial Axial Flow Compressors",
27. Palaghian, L., Bucşă, M. and Ciortan, S., "Pitting corrosion as source of initial fatigue crack",

An Outrun Competition of Corrosion Fatigue and Stress Corrosion Cracking on Crack Initiation in a Compressor Blade

E. Poursaeidi, O. Pedram

Department of Mechanical Engineering, University of Zanjan, Zanjan, Iran

P A P E R I N F O

Paper history:
Received 25 June 2013
Received in revised form 24 August 2013
Accepted 07 November 2013

Keywords:
Corrosion Pitting
Gas Turbine Compressor Blade
Stress Corrosion Cracking
Custom 450

چکیده

پره‌های متحرک ردیف اول چهار کمپرسور جریان محوری به‌طور ناگهانی شکسته شدند. بازرسی‌های گذشته نشان داد که جو محل (محیط کار)، حاوی اجزای خورنده است که موجب افزایش امکان ایجاد حفره بر پره‌ها می‌شود. مشخص شده است که ترک از دو حفره‌ی خوردگی ایجاد گردیده است. این مقاله مشخص می‌کند که کدام یک از سازوکارهای ترک خوردگی تنشی یا خستگی خوردگی، در انتقال حفره‌ها به ترک اولیه غالب است. بدین منظور مطالعات آزمایشگاهی، عددی و نظری انجام شد. بررسی‌های رپلیکا، میکروسکوپ الکترونی روبشی و شکست‌نگاری پره‌ی شکسته شده، نشان داد که حفره‌ها تحت سازوکار ترک خوردگی تنشی به هم متصل شده‌اند و یک حفره‌ی بزرگ‌تر را ساخته‌اند که این موجب کاهش بیشتر زمان شکست می‌شود. مدل‌های سه بعدی حفره بر پره تحت نیروهای موجود با نرم‌افزار آباکوس تحلیل شده است. نتایج شبیه‌سازی، محل تمرکز تنش بیشینه را داخل یکی از حفره‌ها مشخص می‌کند که با محل ترک خوردگی تنشی اولیه هم‌خوانی دارد. تحلیل نظری و عددی بیان می‌دارد که محدوده ی فاکتور شدت تنش در اطراف حفره‌ها کوچک‌تر از محدوده‌ی فاکتور شدت تنش آستانه است؛ بنابراین ترک‌ها از دهانه‌ی حفره تحت سازوکار ترک خوردگی تنشی، ایجاد و منتشر شده و سپس حفره‌ها به‌هم متصل می‌شوند و یک حفره‌ی معادل را می‌سازند، از این رو محدوده ی فاکتور شدت تنش به محدوده ی فاکتور شدت تنش آستانه رسیده و ترک تحت سازوکار خستگی رشد می‌کند.

doi: *10.5829/idosi.ije.2014.27.05b.15*